Three-dimensional femtosecond laser nanolithography of laser crystals

Airán Ródenas[1]*, Min Gu[2], Giacomo Corrielli[1], Petra Paiè[1], Sajeev John[3], Ajoy K. Kar[4], Roberto Osellame[1]

[1]Istituto di Fotonica e Nanotecnologie, Consiglio Nazionale delle Ricerche, Piazza Leonardo da Vinci, 32, I-20133 Milano, Italy.

[2]Laboratory of Artificial-Intelligence Nanophotonics, School of Science, Royal Melbourne Institute of Technology, GPO Box 2476, Melbourne, VIC 3001, Australia

[3]Department of Physics, University of Toronto, 60 St. George Street, Toronto, Ontario, Canada M5S 1A7

[4]Institute of Photonics and Quantum Sciences, David Brewster Building, Heriot-Watt University, Edinburgh, EH14 4AS, UK

*Correspondence to: arodenas@gmail.com

Abstract: Nanostructuring hard optical crystals has so far been exclusively feasible at their surface, as stress induced crack formation and propagation has rendered high precision volume processes ineffective. We show that the inner chemical etching reactivity of a crystal can be enhanced at the nanoscale by more than five orders of magnitude by means of direct laser writing. The process allows to produce cm-scale arbitrary three-dimensional nanostructures with 100 nm feature sizes inside large crystals in absence of brittle fracture. To showcase the unique potential of the technique, we fabricate photonic structures such as sub-wavelength diffraction gratings and nanostructured optical waveguides capable of sustaining sub-wavelength propagating modes

inside yttrium aluminum garnet crystals. This technique could enable the transfer of concepts from nanophotonics to the fields of solid state lasers and crystal optics.

Main Text: The optical properties of a material are known to depend not only on its chemistry but also on its sub-wavelength structure. With the inception of the photonic crystal *(1, 2)* and metamaterial *(3, 4)* concepts this idea proved to be key to access a new level of light manipulation beyond what is allowed by the natural optical properties of materials. However, for over three decades of research no technique has been able to reliably nanostructure optical crystals beyond their surface.

Laser lithography as developed by the semiconductor industry is an intrinsic surface processing technique where a photoresist is two-dimensionally (2D) nanostructured with UV light, and, followed by various subtractive and additive processes, enables the mass production of high-quality nanophotonic planar devices *(5, 6)*. Its extension from 2D to 3D was demonstrated two decades ago by means of infrared femtosecond laser pulses to introduce multiphoton absorption at the resist photo-polymerization step *(7)*. This approach prompted seminal demonstrations of lithographically produced 3D photonic crystals for the optical range, first made of pure polymerized material *(8-10)*, and later transferred to silicon and other optical materials by means of further processing steps *(11, 12)*. The technological exploitation of photo-polymerized structures has however proven to be impractical since they cannot be efficiently interfaced with other photonic elements. A remarkable example of the potential of 3D nanostructuring of macroscopic optical materials comes from the field of optical fibers: photonic crystal fibers have delivered functionalities that go far beyond what is feasible with ordinary unstructured glass *(13, 14)* and have revolutionized the areas of nonlinear optics and optical communications *(15-17)*. Yet, their manufacturing in crystalline media has remained elusive due to the difficulty of applying

stack and drawing techniques with crystals. The prospects of directly machining 3D nanostructures by laser-induced dielectric breakdown also led to reports that amorphous and void sub-micron structures can be induced in crystals, although at the cost of imparting high pressure waves which entail extended lattice damage and crack propagation *(18, 19)*. Despite efforts, no method has been reported for the large scale 3D volume nanostructuring of a crystal.

Departing from prevailing approaches, we propose that the inner chemical reactivity of a crystal, given by its wet etch rate, can be locally modified at the nanometer scale by means of multiphoton 3D laser writing (3DLW) in absence of amorphization and crack formation. We show that cm-long empty pore lattices with arbitrary feature sizes at the 100-nm level can be created inside some
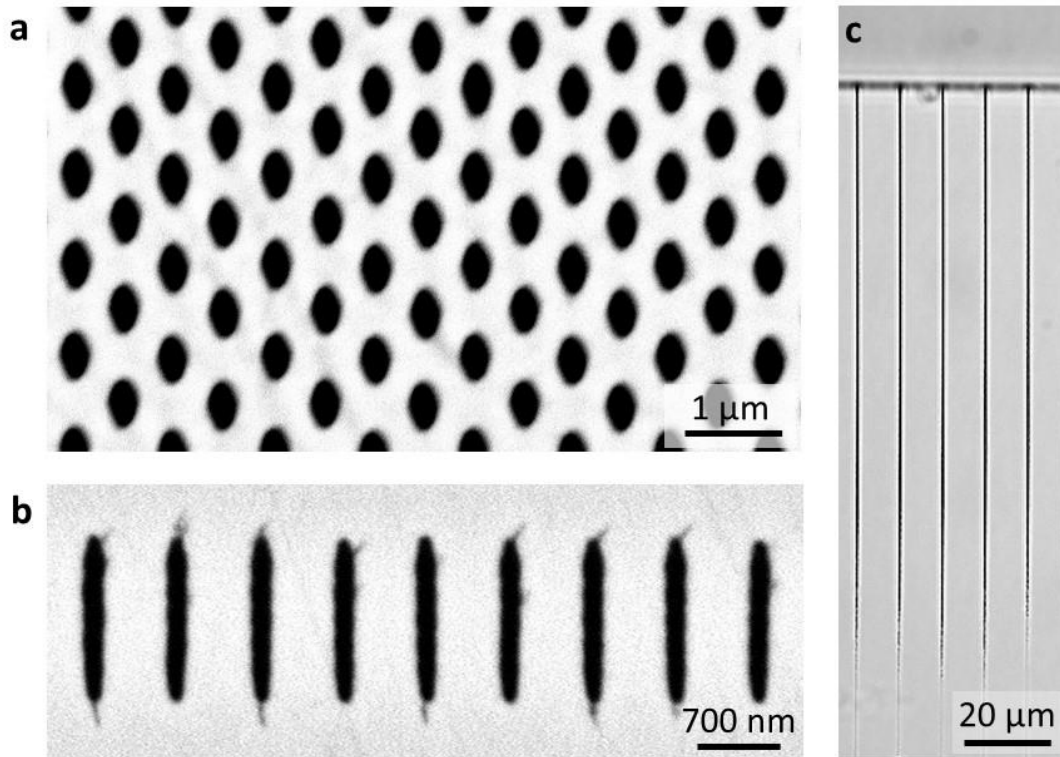

Fig. 1. Wet etching of nanopore lattices fabricated by 3DLW in YAG. (a) Nanopore lattice etched for 120h with average pore size of 257 nm ±7 nm and 454 nm ±13 nm along *x* and *y* reference axes, and 1 mm lengths along *z*. (**b**) Vertically overlapping nanopores after 2h wet etching (average size of 131 nm ±5 nm and 1300 nm ±35 nm, along *x* and *y*, and 1 mm lengths). (**c**) Top optical microscope view of 129 μm ± 6.8 μm long nanopores along *z* direction, etched for 1h.

of the most used crystals in the laser industry (yttrium aluminum garnet and sapphire), in absence of brittle fracture. An etching selectivity larger than 10^5, never observed before in a photo-irradiated material, is achieved between the modified and pristine crystalline states. This allows the design and fabrication of nanophotonic elements inside a crystal that provide optical responses determined by their sub-wavelength structure.

To achieve volume nanostructuring of crystals at large scale it is necessary to arrange nanopores in arbitrary close-packed structures for macroscopic lengths (mm to cm scale) without causing brittle fracture of the crystal due to excessive stress accumulation. In addition, pores have to be written in arbitrary directions, their size must be controlled with at least ~10 nm reproducibility to achieve functional nanophotonic devices, and the pore cross-sectional shape must be tailorable.

We show that all these features (pore direction, size, shape, filling fraction, and length) can be controlled by combining 3DLW and wet etching of YAG crystal. Figure 1 summarizes the controlled creation of nanopore lattices in YAG crystals. No dependence on the crystalline axis was found for the pore size and wet etching rate within our experimental resolution (20), so an arbitrary reference frame is set where x and y axes define the pore's cross sectional plane, and z is defined along the pore length axis. Figure 1a shows a 1 mm long lattice of nanopores arranged in centered orthogonal symmetry with 1 µm in-plane spacing. The lattice was etched for 120 h (20), and the average pore size was of 257 ±7 nm and 454 ±13 nm in x and y directions, respectively. Control over the pore shape and size can be performed by tailoring the laser power and polarization (see Fig. S1), but to achieve bespoke pore shapes for constant laser power the overlapping of pores was also tested. Figure 1b shows an array of parallel pores which were vertically stacked so as to achieve arbitrarily elongated cross-sections. Pores in this experiment were etched for 2h and had an average size of 131 ±5 nm and 1300 ±35 nm along the x and y axes, respectively. The etching

of crossing pores along different directions was also studied to prove the 3D nature of the lithographic process. Figure S2 shows pores that crisscross at 90º angles and at different relative depths within the crystal.

The creation of air pores photonic lattices makes it possible to achieve nanophotonic structures inside the crystal with a spatial resolution equivalent to state-of-the-art multiphoton polymerization lithography [21]. However, the use of nanophotonic devices in practical scenarios requires robust and efficient optical interconnections and capability for the design of large complex circuits. To achieve this, it is essential to keep the spatial resolution and lattice fidelity across large areas on the mm^2 scale or beyond. The critical parameter that limits such control over the pores lengths is the differential etching rate between the photo-modified written volumes and the surrounding pristine crystal. Figure 1c shows a top view optical microscope image of an array of 200 nm nanopores etched for 1h. The large refractive index contrast between air and crystal allow to determine a pore length of ~129 µm and thus an averaged nanopore etch rate of 129 ±6.8 µm/h for the first hour of etching. The slow etching rate of un-modified YAG was determined to be <1 nm/h (0.36 ±0.23 nm/h) from the average of all performed experiments in our wet etching conditions [20]. The 1h average etching selectivity of 3DLW YAG nanopores is thus determined to be greater than 10^5, the highest value ever observed for any lithographic process so far, and approximately two orders of magnitude higher than that of alumina over silicon [22]. Due to this high selectivity, nanopores with cross-sections of 368 x 726 nm^2 and lengths of 3.1 mm were achieved by etching for 170h from both end sides of the pores (see Fig. S3), showing that nanopores with mm-scale lengths are feasible in one single etching step. A similar ultrahigh selectivity and mm-scale nanopore length was also found for sapphire [20]. Furthermore, to homogeneously etch longer nanostructures on the cm scale (or potentially beyond), as well as to keep the etching times as short

as a few hours, a scheme of vertical access etching pores was implemented, thus allowing the achievement of structures with arbitrary length across the whole sample (see Fig. S4).
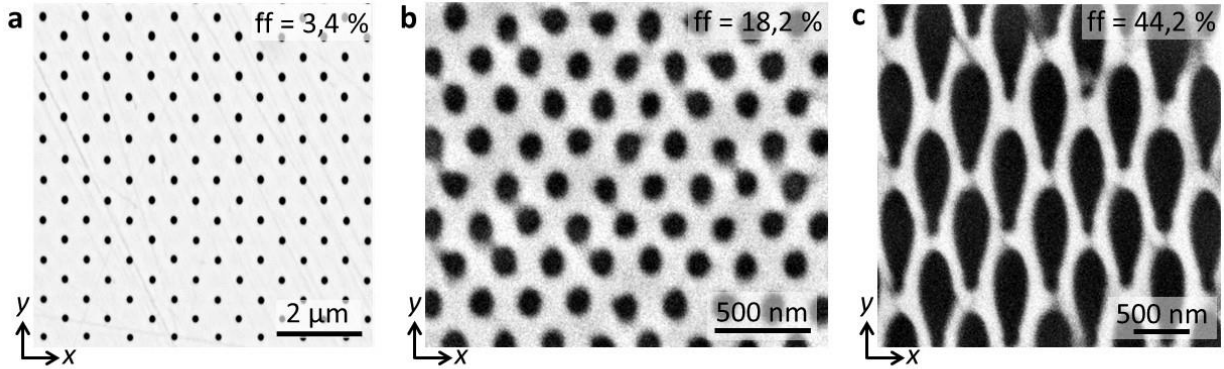

Fig. 2. 3DLW nanostructures with 100 nm feature sizes and filling fraction control. (a) Low pore filling fraction lattice (3,4%) written with linearly varying pore size along depth (top to bottom x-widths ranging from 139±4 nm to 109±6 nm, y-heights from 204±6 nm to 132±8 nm, and aspect ratio from ~1,45 to ~1,20). (b) Hexagonal pore lattice with 250 nm spacing and 18,2% pore filling fraction (average x-width 109 nm ±8 nm, y-height 125 nm ±10 nm, and aspect ratio ~1,15). (c) High filling fraction (44,2%) pore lattice with ~150 nm crystal walls separating elliptical pores with average 276 x 972 nm² cross sections. All pores had ~1 mm lengths.

As shown in Figure 1, the pores cross-sectional aspect ratio can be engineered by means of laser control and pore overlapping, however both these processes inevitably lead to larger pore cross-sections, and for some applications such as the fabrication of photonic crystals and metamaterials in the visible and IR ranges, symmetric pores at the 100 nm level are required. A route to minimizing both the pore size and cross-sectional aspect ratio (i.e. pore height along y-axis divided by width along x-axis) is by performing 3DLW at powers close to the threshold for laser photo-modification. Under our 3DLW experimental conditions *(20)* ~110 nm nanopores were obtained with almost circular shapes for circularly polarized laser irradiation (see Fig. S1). Figure 2a shows a lattice of 1 mm long nanopores fabricated with decreasing powers towards deeper layers. The obtained lattice has a slowly varying pore cross-section with widths ranging from ~139 nm to ~109 nm, heights from ~204 nm down to ~132 nm, and aspect ratios ranging from ~1.45 to ~1.20 at different depths. To test the feasibility of fabricating high filling fraction nanopore lattices without fracturing the crystal, hexagonal lattices with lattice spacing down to 250 nm were fabricated.

Figure 2b shows a close up of such lattice after etching for 15h, with an air filling fraction of 18%, average pore diameter of ~117 nm, aspect ratio of ~1.15, and a dielectric wall thickness of ~133 nm between pores. This control over the lattice spacing down to 250 nm could prove useful for designing 3D photonic band-gap lattices with stopbands ranging from the visible to the mid-IR range *(23)* inside solid state laser crystals such as rare earth ion doped YAG, one of the most used laser materials.

A different route to achieve larger air filling fractions is by etching larger pores. Large air filling fraction structures are also essential for tailoring the properties of microstructured optical waveguides (MOWs) such as the dispersion, mode size and nonlinear coefficient *(13-17)*. Reaching a high air filling fraction inside a crystal requires the fabrication of extended thin crystalline nanolayers without crystal fracture. The creation of such lattices was validated by fabricating a centered orthogonal lattice with in-plane pore spacing of 700 nm and pore cross-sections of 276x972 nm^2 (see Fig. 2c), having a 44% air pore filling fraction and ~150 nm dielectric walls in absence of crack formation even at the surface after mechanical polishing.

Having established the etching rates and achievable features sizes of the crystalline nanostructures inside YAG, we sought to determine whether: (1) the crystal nanopores are indeed void millimeters away from the entrant wet etching surface, and (2) functional sub-wavelength nanophotonics elements on the large scale can indeed be successfully realized. To test the first question, a nanograting with sub-wavelength pitch (700 nm) was fabricated to be tested at 1070 nm wavelength (see Fig. 3a). The sub-wavelength grating was designed to have only one -1st diffraction order (see inset in Fig. 3b), it was fabricated with 10 different laser powers, so as to control the pores cross-sectional shape, and tested in Littrow configuration for the highest diffraction efficiency *(24)*. The highest total efficiency of 86% was obtained for the -1st order of

the grating that had the larger cross-section of the pores, 165 nm width and 1520 nm height. Calculations *(20)* assuming air filled pores are shown in Fig. 3b, agreeing well with the measured values and therefore demonstrating the void nature of the long etched nanopores.
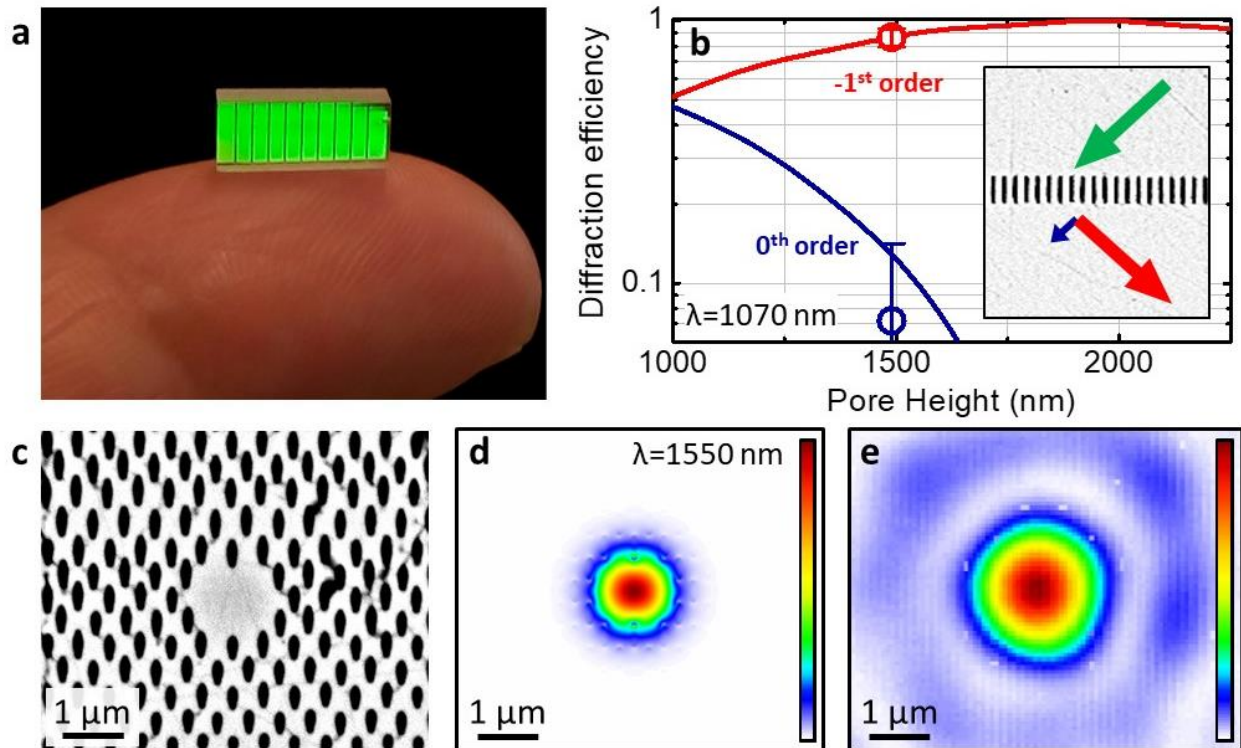

Fig. 3. Sub-wavelength diffraction gratings and MOW (microstructured optical waveguide). (**a**) Image of a cm-long 700 nm pitch grating under visible light illumination. (**b**) Experimental and calculated diffraction efficiency of a 700 nm pitch sub-wavelength grating for 1070 nm wavelength. Inset shows a SEM close up of the fabricated grating. (**c**) Optical waveguide with hexagonal structure, 500 nm horizontal pore-to-pore spacing, mean pore size of 166 x 386 nm^2 and 4 mm length. (**d**) Simulated intensity mode profile at 1550 nm with FWHM of 862 nm (vertical) and 972 nm (horizontal). (**e**) Diffraction-limited near-field image of the waveguide output mode measured at 1550 nm wavelength, with a FWHM of ~1,5 μm.

To further evaluate the quality and potential of the crystal 3D nanolithography technique, the fabrication of MOWs with different lattice spacings and cavity sizes was studied (see Fig. S5). Figure 3c shows a nanostructured waveguide with core size of 1.1 x 1.3 μm^2, a triangular symmetry cladding with in-plane spacing of 500 nm, an average pore size of 166 x 386 nm^2, and a length of

4 mm. Figure 3d shows the theoretical mode at 1550 nm wavelength for vertically polarized electric field, as calculated by means of finite element method (FEM). The mode is effectively sub-wavelength having a full width at half maximum (FWHM) of ~900 nm (~0.6λ). Figure 3e shows the measured diffraction-limited *(20)* image of the waveguide output mode for vertical polarization at 1550 nm. From the FEM computations the MOW is expected to have a modified dispersion function with two theoretical zero dispersion wavelengths (ZDW) at 0.93 µm and 1.51 µm wavelength (see Fig. S6), well below the natural ZDW of YAG at 1.6 µm, which could allow for ultrafast nonlinear supercontinuum generation with standard commercial Nd^{3+} and Yb^{3+} short pulse lasers *(15)*.

Besides the novel applications on crystalline 3D nanophotonics and nonlinear optics, to which this technique gives a large impetus, the 3D structuring of YAG laser crystals also opens up new ways to overcome current limitations in the design of compact solid-state rare-earth-doped lasers, such as for the integration of traditional cavity elements (e.g. mirrors, dispersion control elements, microfluidic cooling channels) directly in the gain media itself with expected improvements in compactness, robustness and performance of the devices. The possibility of fabricating large nanostructured YAG laser crystals with reduced surface defects due to the wet etching process also opens up potential for new applications in ultra-strong deformable laser nanofibers *(25-27)*.

References and Notes:

1. S. John, Strong localization of photons in certain disordered dielectric superlattices. *Phys. Rev. Lett.* **58**, 2486 (1987). doi: 10.1103/PhysRevLett.58.2486

2. E. Yablonovitch, Inhibited Spontaneous Emission in Solid-State Physics and Electronics. *Phys. Rev. Lett*. **58**, 2059 (1987). doi:10.1103/PhysRevLett.58.2059

3. R. A. Shelby, D. R. Smith, S. Schultz, Experimental verification of a negative index of refraction. *Science* **292**, 5514, 77-79 (2001). doi:10.1126/science.1058847

4. D. R. Smith, J. B. Pendry, M. C. K. Wiltshire, Metamaterials and negative refractive index. *Science* **305**, 5685, 788-792 (2004). doi: 10.1126/science.1096796

5. K. Jain, C. G. Willson, B.J. Lin, Ultrafast deep UV lithography with excimer lasers. *IEEE Electron Device Lett*. **3**, 3, 53-55 (1982). doi:10.1109/EDL.1982.25476

6. K. McGarvey-Lechable, T. Hamidfar, D. Patel, L. Xu, D. V. Plant, P. Bianucci, Slow light in mass-produced dispersion-engineered photonic crystal ring resonators. *Opt. Express* **25**, 3916-3926 (2017). doi:10.1364/OE.25.003916

7. S. Maruo, O. Nakamura, S. Kawata, Three-dimensional microfabrication with two-photon-absorbed photopolymerization. *Opt. Lett.* **22**, 132-134 (1997). doi:10.1364/OL.22.000132

8. M. Straub, M. Gu, Near-infrared photonic crystals with higher-order bandgaps generated by two-photon photopolymerization. *Opt. Lett.* **27**, 1824-1826 (2002). doi:10.1364/OL.27.001824

9. M. Deubel, G. von Freymann, M. Wegener, S. Pereira, K. Busch, C. M. Soukoulis, Direct laser writing of three-dimensional photonic-crystal templates for telecommunications. *Nat. Mater.* **3**, 444-447 (2004). doi:10.1038/nmat1155

10. S. Wong, M. Deubel, F. Pérez-Willard, S. John, G. A. Ozin, M. Wegener, G. von Freymann, Direct Laser Writing of Three- Dimensional Photonic Crystals with a Complete Photonic Bandgap in Chalcogenide Glasses. *Adv. Mater.* **18**, 3, 265-269 (2006). doi: 10.1002/adma.200501973

11. M. Hermatschweiler, A. Ledermann, G. A. Ozin, M. Wegener, G. von Freymann, Fabrication of silicon inverse woodpile photonic crystals. *Adv. Funct. Mater.* **17**, 14, 2273-2277 (2007). doi:10.1002/adfm.200601074

12. J. K. Gansel, M. Thiel, M. S. Rill, M. Decker, K. Bade, V. Saile, G. von Freymann, S. Linden, M. Wegener. Gold Helix Photonic Metamaterial as Broadband Circular Polarizer. *Science* **325**, 1513 (2009). doi:10.1126/science.1177031

13. J. C. Knight, T. A. Birks, P. St. J. Russell, D. M. Atkin, All-silica single-mode optical fiber with photonic crystal cladding. *Opt. Lett.* **21**, 1547-1549 (1996). doi:10.1364/OL.21.001547

14. P. Russell, Photonic Crystal Fibers. *Science* **299**, 5605, 358-363 (2003). doi:10.1126/science.1079280

15. J. M. Dudley, G. Genty, S. Coen. Supercontinuum generation in photonic crystal fiber. *Rev. Mod. Phys.* **78**, 1135–1184 (2006). doi:10.1103/RevModPhys.78.1135

16. J. G. Rarity, J. Fulconis, J. Duligall, W. J. Wadsworth, P. St. J. Russell, Photonic crystal fiber source of correlated photon pairs. *Opt. Express* **13**, 534-544 (2005). doi:10.1364/OPEX.13.000534

17. R. J. A. Francis-Jones, R. A. Hoggarth, P. J. Mosley, All-fiber multiplexed source of high-purity single photons. *Optica* **3**, 1270-1273 (2016). doi:10.1364/OPTICA.3.001270

18. E. N. Glezer, E. Mazur, Ultrafast-laser driven micro-explosions in transparent materials. *Appl. Phys. Lett.* **71**, 882 (1997). doi:10.1063/1.119677

19. S. Juodkazis, K. Nishimura, H. Misawa, T. Ebisui, R. Waki, S. Matsuo, T. Okada, Control over the crystalline state of sapphire. *Adv. Mater.* **18**, 11, 1361-1364 (2006). doi:10.1002/adma.200501837

20. Materials and methods are available in the Supplementary Information.

21. J. Fischer, J. B. Mueller, J. Kaschke, T. J. A. Wolf, A.-N. Unterreiner, M. Wegener, Three-dimensional multi-photon direct laser writing with variable repetition rate. *Opt. Express* **21**, 26244-26260 (2013). doi:10.1364/OE.21.026244

22. M. D. Henry, S. Walavalkar, A. Homyk, A. Scherer, Alumina etch masks for fabrication of high-aspect-ratio silicon micropillars and nanopillars. *Nanotechnology* **20**, 25 (2009). doi:10.1088/0957-4484/20/25/255305

23. J. D. Joannopoulos, P. R. Villeneuve, S. Fan, Photonic crystals: putting a new twist on light. *Nature*, **386**, 143-149 (1997). doi:10.1038/386143a0

24. T. Clausnitzer, T. Kämpfe, E.-B. Kley, A. Tünnermann, A. V. Tishchenko, O. Parriaux, Highly-dispersive dielectric transmission gratings with 100% diffraction efficiency. *Opt. Express* **16**, 5577-5584 (2008). doi:10.1364/OE.16.005577

25. L. R. Meza, S. Das, J. R. Greer, Strong, lightweight, and recoverable three-dimensional ceramic nanolattices. *Science* **345**, 6202, 1322-1326 (2014). doi:10.1126/science.1255908

26. J. Bauer, A. Schroer, R. Schwaiger, O. Kraft, Approaching theoretical strength in glassy carbon nanolattices. *Nat. Mater.* **15**, 438-443 (2016). doi:10.1038/nmat4561

27. A. Banerjee, D. Bernoulli, H. Zhang, M.-F. Yuen, J. Liu, J. Dong, F. Ding, J. Lu, M. Dao, W. Zhang, Y. Lu, S. Suresh. Ultralarge elastic deformation of nanoscale diamond. *Science* **360**, 6386, 300-302 (2018). doi:10.1126/science.aar4165

Competing interests: Non declared.

Data and materials availability: All data needed to evaluate the conclusions is available in the main text or the supplementary materials.